J Mater Sci (2009) 44:926–930
DOI 10.1007/s10853-008-3192-y

Preparation of γ-Fe_2O_3 nanopowders by direct thermal decomposition of Fe-urea complex: reaction mechanism and magnetic properties

S. Zhao · H. Y. Wu · L. Song · O. Tegus · S. Asuha

Received: 2 July 2008 / Accepted: 12 December 2008 / Published online: 31 December 2008

Abstract In this work, a novel method of producing maghemite (γ-Fe_2O_3) nanopowders has been developed, which can be performed by the direct thermal decomposition of an Fe–urea complex ($[Fe(CON_2H_4)_6](NO_3)_3$) in a single step. The reaction mechanism, particle morphology, and the magnetic properties of the γ-Fe_2O_3 nanopowders have been studied by using thermogravimetric (TG), differential scanning calorimetry (DSC), fourier transformed infrared (FTIR) spectroscopy, elemental analysis, X-ray powder diffraction (XRD), transmission electron micrograph (TEM) observations, and magnetic measurements. Thermal analyses together with the results of XRD show that the formation of γ-Fe_2O_3 occurs at $\sim$200 °C through a two-stage thermal decomposition of the $[Fe(CON_2H_4)_6](NO_3)_3$ complex. The resulting iron oxide phases (i.e., γ-Fe_2O_3 and α-Fe_2O_3) are strongly dependent on the synthesis conditions of the $[Fe(CON_2H_4)_6](NO_3)_3$. When the molar ratio of $Fe(NO_3)_3 \cdot 9H_2O$ to CON_2H_4 that is used for the synthesis of $[Fe(CON_2H_4)_6](NO_3)_3$ is 1:6 (i.e., molar ratio in stoichiometry), a mixed phase of γ-Fe_2O_3 and α-Fe_2O_3 is formed. When the molar ratio is 1:6.2 (i.e., using an excess CON_2H_4), on the other hand, a pure γ-Fe_2O_3 is obtained. Magnetic measurements show that resulting nanopowders exhibit a ferromagnetic characteristic and their maximum saturation magnetization increases from 47.2 to 67.4 emu/g with an increase in the molar ratio of $Fe(NO_3)_3 \cdot 9H_2O$ to CON_2H_4 from 1:6 to 1:6.2.

S. Zhao · H. Y. Wu · S. Asuha (✉)
Chemistry & Environment Science College, Inner Mongolia Normal University, Key Laboratory of Physics and Chemistry of Function Materials, Inner Mongolia, 81 Zhaowudalu, Hohhot 010022, China
e-mail: asuha42@yahoo.com.cn

L. Song · O. Tegus
Physics & Electronic Information College, Inner Mongolia Normal University, Key Laboratory of Physics and Chemistry of Function Materials, Inner Mongolia, 81 Zhaowudalu, Hohhot 010022, China

Introduction

Magnetic nanoparticles are now of interest because of their unique magnetic properties and many applications [1, 2]. Iron oxides are the mostly used magnetic materials because they are chemically stable under various conditions. In iron oxide crystalline forms, γ-Fe_2O_3 is a ferromagnetic material, and it has already been extensively used as a magnetic recording material for a long time [3]. Besides this, it is also widely used in drug delivery [4], catalysis [5], magneto-optical device [6], ferro-fluids [7], and magnetic refrigeration [8]. In recent years, the γ-Fe_2O_3 attracts much attention from environmental applications in which it is used as a magnetic support of photocatalysts as well as a photocatalyst [9, 10]. For all of these applications, pure and high quality γ-Fe_2O_3 nanopowders are required to satisfy new increasing demands. Therefore, the preparation of γ-Fe_2O_3 nanopowders now attracts a lot of interest and various methods have been developed. The conventional hydrolytic synthetic method of γ-Fe_2O_3 powder using ferrous salts as starting materials involves three or more steps. In the case of production of acicular γ-Fe_2O_3 powder that is used for magnetic tapes, for example, usually five steps are needed. In addition, the agglomeration of particles is easy to occur in the aqueous solution, and therefore usually a capping agent is needed to prevent the particle agglomeration [11]. In some aqueous synthetic methods such as sol-gel process where inorganic salts of iron (e.g.,

$Fe(NO_3)_3 \cdot 9H_2O$) are used as precursors, hematite (α-Fe_2O_3), an antiferromagnetic material, is always produced as an accompanying phase [12–15]. Attention has therefore been focused on the development of nonaqueous synthetic methods, and shape and size-controlled high quality γ-Fe_2O_3 nanopowders have been successfully prepared using an iron-pentacarbonyl ($Fe(CO)_5$) as a source of iron [16, 17]. However, although $Fe(CO)_5$ is commonly used as a precursor in many nonaqueous processes and the oxidative pyrolysis of which can form γ-Fe_2O_3 nanopowders, its toxic and unstable property may limit the usage of these methods for the mass production of γ-Fe_2O_3 nanopowders.

As an easy synthetic process, pyrolytic method attracts much attention mainly from their simplicity and low cost, and several kinds of methods have been investigated to prepare γ-Fe_2O_3 nanopowders, e.g., direct combustion pyrolysis [18], spray pyrolysis [19], flame pyrolysis [20, 21], etc. However, the Fe-containing precursors whose pyrolysis can directly produce γ-Fe_2O_3 nanopowders are limited to few relatively rare iron complexes such as $N_2H_5Fe(N_2H_3COO)_3 \cdot H_2O$, $Fe(N_2H_3COO)_2(N_2H_4)_2$, and $Fe(C_5H_5)_2$. Inorganic salts of iron (e.g., ferric nitrate) also can be used as a precursor, but in this case a fuel (e.g., glycine, hydrazine) is necessary to produce γ-Fe_2O_3 nanopowders [22].

In the present study, we have developed a novel method by which the γ-Fe_2O_3 nanopowders can be prepared in a single step. In this method, $[Fe(CON_2H_4)_6](NO_3)_3$ is directly thermally decomposed at temperature $\sim$200 °C in air to form γ-Fe_2O_3 nanopowders. Since $[Fe(CON_2H_4)_6](NO_3)_3$ is a commercially available chemical, therefore we call this method as one-step method. Main advantages of this method are: (i) the preparation procedure is very simple, (ii) the $[Fe(CON_2H_4)_6](NO_3)_3$ is a nontoxic commercially available chemical, as well as can be easily synthesized from readily available $Fe(NO_3)_3 \cdot 9H_2O$ and CON_2H_4, and (iii) the preparation temperature (i.e., the thermal decomposition temperature of $[Fe(CON_2H_4)_6](NO_3)_3$) is as low as $\sim$200 °C, which is desirable for the formation of pure γ-Fe_2O_3 since it tends to transform into more stable α-Fe_2O_3 at a high temperature above 400 °C. These advantages mean the method does not need an expensive and complicated unit to produce γ-Fe_2O_3 nanopowders, and the low preparation temperature can prevent the γ-Fe_2O_3 nanopowders from agglomeration and phase transformation.

Experimental procedure

Preparation

The preparation of γ-Fe_2O_3 nanopowders starts from the synthesis of $[Fe(CON_2H_4)_6](NO_3)_3$ as follows: firstly, $Fe(NO_3)_3 \cdot 9H_2O$ and CON_2H_4 were mixed in given molar ratio in ethanol at room temperature, followed by intensely stirring until the reactants were completely converted to a light green powder (i.e. $[Fe(CON_2H_4)_6](NO_3)_3$). Then the powder was separated from ethanol by filtering and rinsed with ethanol several times. The formation of $[Fe(CON_2H_4)_6](NO_3)_3$ was confirmed using Fourier transformed infrared (FTIR) spectroscopy and chemical elemental analysis. After drying in an oven at 45 °C for 1 day, the $[Fe(CON_2H_4)_6](NO_3)_3$ powder was heated in air to 200 °C and held at this temperature for 1 h, resulting in the formation of a red-brown fine γ-Fe_2O_3 powder. In order to investigate the effect of the combination ratio of $Fe(NO_3)_3 \cdot 9H_2O$ and CON_2H_4 that are used for the synthesis of $[Fe(CON_2H_4)_6](NO_3)_3$ on the resulting iron oxide phases, two kinds molar ratios of $Fe(NO_3)_3 \cdot 9H_2O$ to CON_2H_4, i.e., 1:6.0 (labeled A) and 1:6.2 (labeled B), were investigated.

Characterization

FTIR spectra were recorded using a Nicolet Nexus 670 spectrometer in a dry-nitrogen atmosphere. Elemental analyses were carried out using an Elementar vario EL III elemental analyzer. Thermogravimetric analysis (TG) and differential scanning calorimetry (DSC) measurements were carried out on a NETZSCH STA 409 PC/PG thermal analyzer in air. X-ray powder diffraction (XRD) patterns were recorded on a Philips PW 1830 diffractometer using CuKα radiation. TEM was recorded using a JEOL JEM-3000F transmission electron microscope. Magnetic measurements were performed using a Lake Shore 7407 vibrating-sample magnetometer (VSM) at room temperature.

Results and discussion

Synthesis of $[Fe(CON_2H_4)_6](NO_3)_3$

Figure 1 shows the infrared spectra of CON_2H_4 (spectrum a) and the powder obtained via mixing $Fe(NO_3)_3 \cdot 9H_2O$ and CON_2H_4 in the molar ratio of 1:6.2 (spectrum b). In comparison with spectrum (a), the following four large changes were clearly observed in the spectrum (b): (1) the absorption band at 1686 cm^{-1}, which was attributable to C=O stretching vibration, shifted to 1629 cm^{-1}, (2) the band at 1466 cm^{-1}, which was attributable to C–N stretching vibration, shifted to 1499 cm^{-1}, (3) the band at 3206 cm^{-1}, which was due to N–H stretching vibration, increased its intensity, and (4) a new strong band was observed at 1385 cm^{-1}, which was a characteristic absorption band of NO^{3-}. The former three changes indicate that the CON_2H_4 molecules are coordinated to the Fe^{3+}; this result together with the absorption band of NO^{3-}

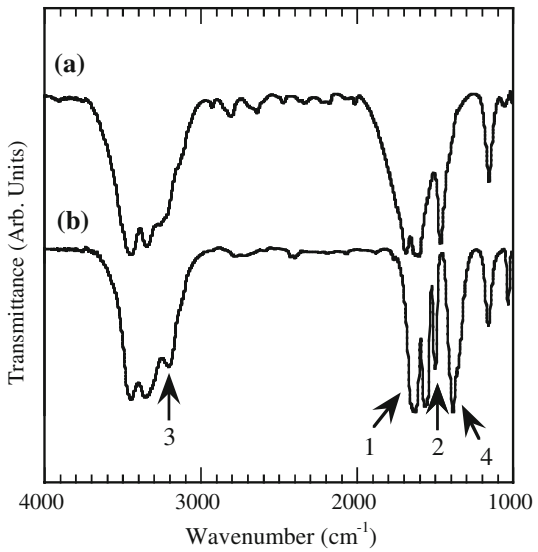

Fig. 1 FTIR spectra: (a) for the urea and (b) for the $[Fe(CON_2H_4)_6](NO_3)_3$ synthesized from $Fe(NO_3)_3 \cdot 9H_2O$ and CON_2H_4

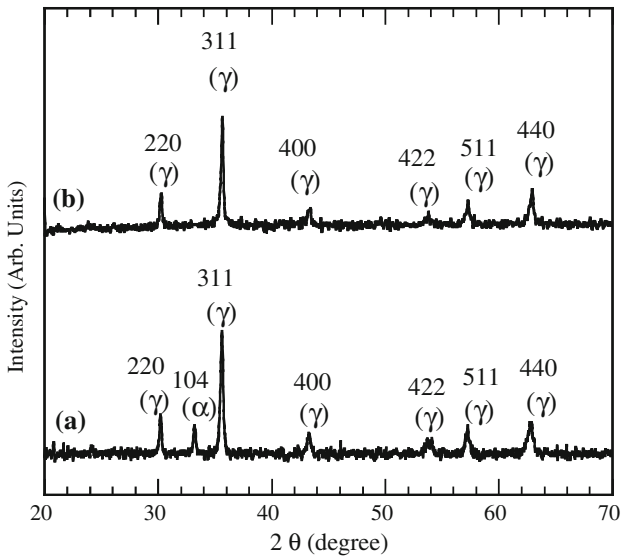

Fig. 2 XRD patterns for the samples prepared by the thermal decomposition of $[Fe(CON_2H_4)_6](NO_3)_3$ that is synthesized from different molar ratios of $Fe(NO_3)_3 \cdot 9H_2O$ to CON_2H_4 at 200 °C: (a) 1:6 (sample A) and (b) 1:6.2 (sample B)

Table 1 Contents of N, C, and H in the complex synthesized from iron nitrate and urea

Content (%)		
N	C	H
35.28[a]	12.47[a]	4.28[a]
34.89[b]	11.97[b]	4.02[b]

[a] Experimental value

[b] Calculated value

suggest the formation of $[Fe(CON_2H_4)_6](NO_3)_3$ complex [23]. The result of elemental analysis of the complex is shown in Table 1. The contents of Fe, C, N, and H were in good agreement with their calculated values. This further confirms the formation of $[Fe(CON_2H_4)_6](NO_3)_3$.

Formation of γ-Fe_2O_3 nanopowders

Figure 2 shows the XRD patterns of the samples prepared by the thermal decomposition of $[Fe(CON_2H_4)_6](NO_3)_3$ at 200 °C. Patterns (a) and (b) were for the samples A and B, respectively. In the case of sample A, besides one peak appeared at 33.2° (2θ), which was attributable to α-Fe_2O_3, all diffraction peaks were due to γ-Fe_2O_3, showing the formation of a mixed phase of γ-Fe_2O_3 and α-Fe_2O_3. For the sample B, on the other hand, no diffraction peak of α-Fe_2O_3 was observed, and the diffraction pattern matches well with the JCPDS file of γ-Fe_2O_3 (e.g., No. 39-1346), indicating the formation of pure γ-Fe_2O_3 with a cubic spinel crystalline structure. The d-spacing values of the sample B with those of standard γ-Fe_2O_3 and Fe_3O_4 in the JCPDS files are listed in Table 2. From the result, the lattice constant was estimated to be 8.352 Å, which is in well agreement with that of standard γ-Fe_2O_3. The average crystallite size of γ-Fe_2O_3, which was calculated from the half-width of diffraction liens by using Scherrer's equation, was about 24 nm. Fe_3O_4 also possesses a cubic spinel crystalline structure, but the XRD result obtained in the present work differs from its JCPDS file, as shown in Table 2.

Table 2 d-Spacings of the sample B and those of γ-Fe_2O_3 and Fe_3O_4 from JCPDS files

Sample B (Å)	γ-Fe_2O_3 (Å) (JCPDS No. 39-1346)	Fe_3O_4 (Å) (JCPDS No. 19-629)	*hkl*
2.9425	2.9530	2.9670	220
2.5137	2.5177	2.5320	311
2.0866	2.0866	2.0993	400
1.7033	1.7045	1.7146	422
1.6058	1.6073	1.6158	511
1.4745	1.4758	1.4845	440

The effect of the molar ratio of $Fe(NO_3)_3 \cdot 9H_2O$ to CON_2H_4 on the resulting iron oxide phases can be explained from the formation and the dissociation reactions of the $[Fe(CON_2H_4)_6](NO_3)_3$ complex:

$$Fe^{3+} + 6CON_2H_4 + 3NO_3^- \rightleftharpoons \left[Fe(CON_2H_4)_6\right](NO_3)_3 \quad (1)$$

When the complex formation reaction proceeds in stoichiometrically (i.e., $Fe(NO_3)_3 \cdot 9H_2O$: CON_2H_4 = 1:6.0 mole; sample A), a free Fe^{3+} ion is still present in the

solution because of the reverse reaction (i.e., the dissociation reaction of the $[Fe(CON_2H_4)_6](NO_3)_3$) although the complex is very stable. According to the previous work, this free Fe^{3+} ion is easily hydrolyzed by the water from $Fe(NO_3)_3 \cdot 9H_2O$ to form $Fe(OH)_3$, and the dehydration of $Fe(OH)_3$ on subsequent heat treating process results in the formation of α-Fe_2O_3 [24]. Therefore, we think that the presence of a free Fe^{3+} ion is the most probable reason for the formation of α-Fe_2O_3 in the sample A. In the case of sample B, however, the reverse reaction is likely to be completely suppressed by using an excess of CON_2H_4, which further avoids the formation of α-Fe_2O_3; consequently, a pure γ-Fe_2O_3 is formed.

Figure 3 shows the TG-DSC curves of the $[Fe(CON_2H_4)_6](NO_3)_3$. The TG curve showed a two-stage weight loss where the first stage occurred in the range 180–196 °C (denoted by (I) in the figure) and the second in the range 196–280 °C (denoted by (II) in the figure), indicating a two-stage thermal decomposition mechanism. The weight losses for the first and the second stage were 60.6 and 25.1%, respectively; the total weight loss was 85.8%. On the basis of this two-stage

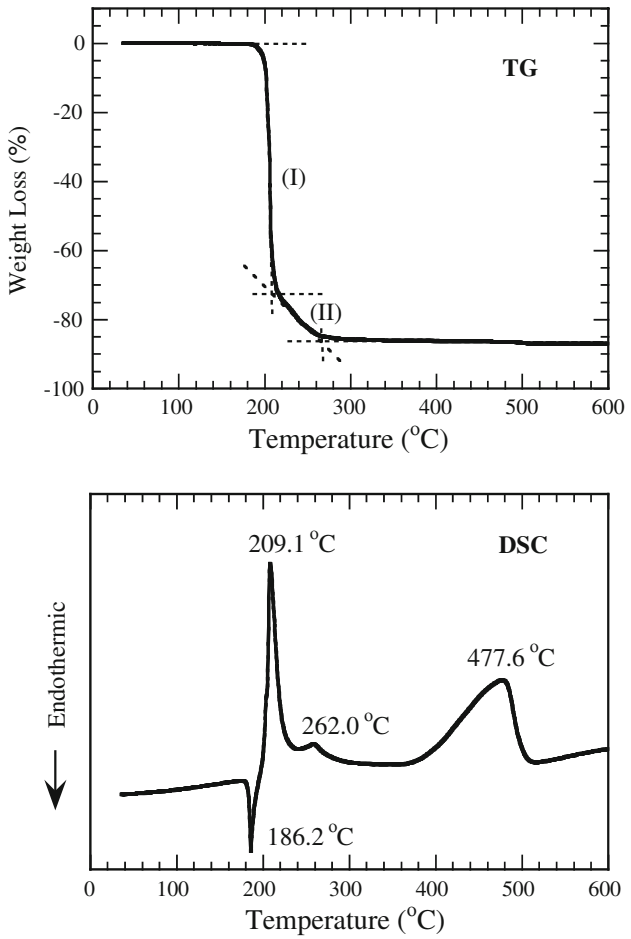

Fig. 3 TG-DSC curves for the $[Fe(CON_2H_4)_6](NO_3)_3$ synthesized from $Fe(NO_3)_3 \cdot 9H_2O$ and CON_2H_4

weight loss, the following stoichiometric decomposition reactions are proposed.

$$[Fe(CON_2H_4)_6](NO_3)_3 \rightarrow Fe(NO_3)_3 + 6CON_2H_4 \quad \text{(first stage)} \tag{2}$$

$$Fe(NO_3)_3 \rightarrow 1/2Fe_2O_3 + 1.5NO + 1.5NO_2 + 3/2O_2 \quad \text{(second stage)} \tag{3}$$

According to these decomposition reactions, the total weight loss for the thermal decomposition was calculated to be 86.7%; hence, the above experimentally obtained total weight loss was in well agreement with the calculated value within an allowable experimental error of 1%.

Four large thermochemical behaviors were observed in the DSC curve. The endothermic peak at ~186 °C was due to the melting of $[Fe(CON_2H_4)_6](NO_3)_3$. From this, the melting point of the complex was estimated to be ~180 °C, which is well consistent with the reported value. The two exothermic peaks at ~209 and ~262 °C were attributable to the first stage and the second stage decompositions of $[Fe(CON_2H_4)_6](NO_3)_3$, respectively. The one broad and strong exothermic peak at ~478 °C was due to phase transformation from γ-Fe_2O_3 to α-Fe_2O_3.

Based on these results of thermal analyses together with those of XRD, it can be concluded that the formation of γ-Fe_2O_3 nanopowders occurs at ~200 °C through a two-stage thermal decomposition of $[Fe(CON_2H_4)_6](NO_3)_3$.

Figure 4 shows the TEM micrograph of γ-Fe_2O_3 nanopowders (sample B). It is clearly seen that the shape of the γ-Fe_2O_3 particles were spherical, and their average particle size was ~20 nm, which was in approximate agreement with that obtained from XRD. A slight particle agglomeration was observed, probably due to the higher surface

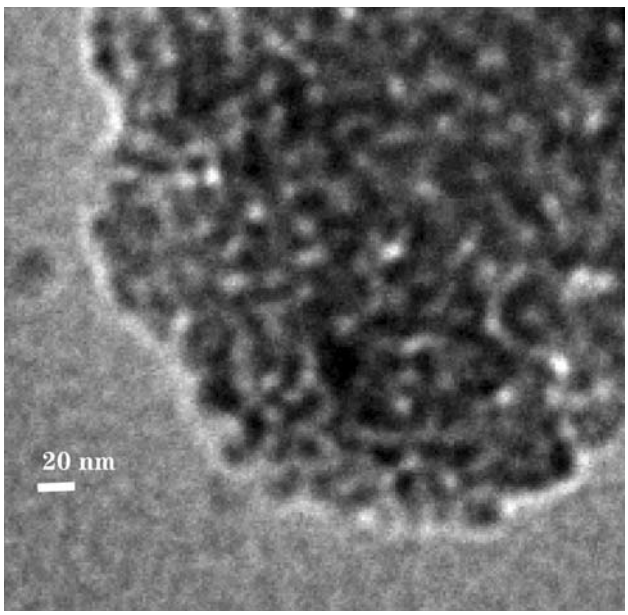

Fig. 4 TEM micrograph of γ-Fe_2O_3 nanopowders (sample B)

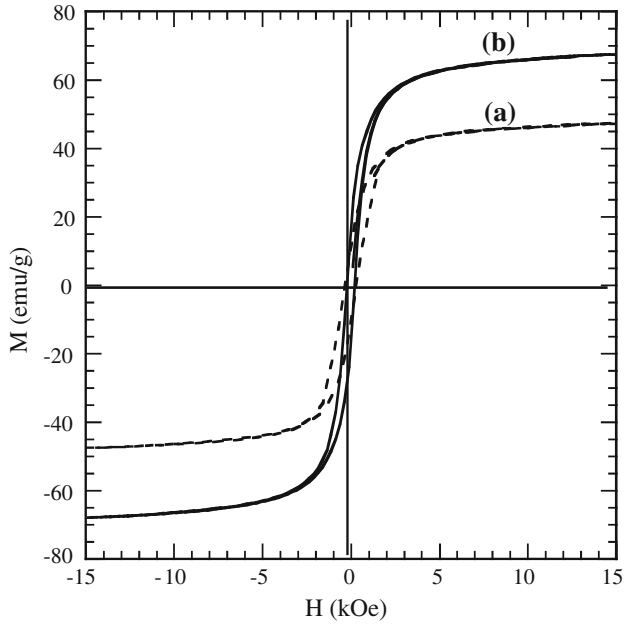

Fig. 5 Magnetization curves for the samples prepared by the thermal decomposition of $[Fe(CON_2H_4)_6](NO_3)_3$ that is synthesized from different molar ratios of $Fe(NO_3)_3 \cdot 9H_2O$ to CON_2H_4 at 200 °C: (a) 1:6 (sample A) and (b) 1:6.2 (sample B)

energy of the nanopowders or to the magnetic interaction of particles.

Magnetic Properties of γ-Fe_2O_3 nanopowders

Figure 5 shows the magnetization hysteresis curves of the samples prepared by the thermal decomposition of $[Fe(CON_2H_4)_6](NO_3)_3$ at 200 °C. Curves (a) and (b) were for the samples A and B, respectively. Both samples exhibited typical ferromagnetic characteristics with a relatively large coercivity (e.g., 212 Oe for Sample B) and remanent magnetization (e.g., 16.8 emu/g for Sample B). A large difference in saturation magnetization (Ms) between the two samples was observed; i.e., the Ms of sample A was considerably smaller than that of sample B. As confirmed from the result of XRD, an antiferromagnetic α-Fe_2O_3 phase is present in the sample A; hence, the presence of α-Fe_2O_3 is thought to be a main reason for the reduction of Ms. For the sample B, Ms was 67.5 emu/g, which is slightly smaller than that of bulk γ-Fe_2O_3 crystallite (i.e., 73.5 emu/g). This discrepancy has also been reported by other researchers [25, 26], and it is likely due to the surface spin canting effects [27].

Conclusions

In this work, we have developed a novel method to prepare pure γ-Fe_2O_3 nanopowders using the direct thermal decomposition of $[Fe(CON_2H_4)_6](NO_3)_3$. In this method, pure γ-Fe_2O_3 nanopowders can be obtained in a single step. The resulting iron oxide phases are dependent on the molar ratio of $Fe(NO_3)_3 \cdot 9H_2O$ to CON_2H_4 that is used for the synthesis of the $[Fe(CON_2H_4)_6](NO_3)_3$. To produce a pure γ-Fe_2O_3, the use of excess CON_2H_4 is desirable for the synthesis of $[Fe(CON_2H_4)_6](NO_3)_3$ complex.

References

1. Yan ZJ, Xue DS (2008) J Mater Sci 43:771. doi:10.1007/s10853-007-2046-3
2. Chen XH, Song HAH (2007) J Mater Sci 42:8738. doi:10.1007/s10853-007-1825-1
3. Dhara S, Rastogi AC, Das BK (1993) J Appl Phys 74:7019
4. Neuberger T, Schöpf B, Hofmann H, Hofmann M, Rechenberg BV (2005) J Magn Magn Mater 293:483
5. Lominicki S, Dellinger B (2003) Environ Sci Technol 37:4254
6. Zayat M, Monte F, Morales MP, Rosa G, Guerrero H, Serna CJ, Levy D (2003) Adv Mater 15(21):1809
7. Grimm S, Schultz M, Barth S, Muller R (1997) J Mater Sci 32:1083. doi:10.1023/A:1018598927041
8. Mcmichael RD, Shull RD, Swartzendruber LJ, Watson RE (1992) J Magn Magn Mater 111:29
9. Chen F, Xie Y, Zhao J, Lu G (2001) Chemosphere 44:1159
10. Apte SK, Naik SD, Sonawane RS, Kale BB (2007) J Am Ceram Soc 90:412
11. Prasad NK, Panda D, Singh S, Mukadam MD, Yusuf SM, Bahadur D (2005) J Appl Phys 97:10Q903
12. Kojima K, Miyazaki M (1997) J Sol-Gel Sci Tech 8:77
13. Cannas C, Concas G, Falgui A, Musinu A, Spano G, Piccaluga G (2001) J Non Cryst Solids 286:64
14. Solinas S, Piccaluga G, Morales MP, Serna CJ (2001) Acta Mater 49:2805
15. Ortega D, Garitaonandia JS, Barrera-Solano C, Bamírez-del-Solar M, Blanco E, Domínguez M (2006) J Non Cryst Solids 352:2801
16. Hyeon T, Lee SS, Park J, Chung Y, Na HB (2001) J Am Chem Soc 123:12798
17. Cheon J, Kang N-J, Lee S-M, Lee J-H, Yoon J-H, Oh SJ (2004) J Am Chem Soc 126:1950
18. Ravindranathan P, Patil KC (1986) J Mater Sci Lett 5:221
19. Li D, Wu D, Zhu J, Wang X, Lu L, Yang X (2003) J Mater Sci Lett 22:931
20. Yang S, Yi J-H, Son S, Jang J, Altman I, Pikhitsa P, Choi M (2003) Appl Phys Lett 83:4842
21. Inamdar SN, Haram SK (2006) J Nanosci Nanotechnol 6:2155
22. Deshpande K, Mukasyan A, Varma A (2004) Chem Mater 16:4896
23. Penland RB, Mizushima S, Curran C, Quagliano JV (1957) J Am Chem Soc 79:1575
24. Nogami M, Asuha N (1993) J Mater Sci Lett 12:1705
25. Woo K, Hong J, Choi S, Lee HW, Ahn JP, Kim CS, Lee SW (2004) Chem Mater 16:2814
26. Jing Z (2006) Mater Lett 60:2217
27. Morales MP, Veitemillas-Verdaguer S, Montero MI, Sema CJ, Roig A, Casas LI, Martínez B, Sandiumenge F (1999) Chem Mater 11:3058